Supplementary Materials

Brittle-to-ductile transition and theoretical strength in a metal-organic framework glass

Shaohua Yan[a,b], Thomas D. Bennett[c], Weipeng Feng[d], Zhongyin Zhu[e], Dingcheng Yang[f], Zheng Zhong[b,*], Qing H. Qin[g,*]

[a] *College of Physics and Optoelectronic Engineering, Shenzhen University, Shenzhen, China.*

[b] *School of Science, Harbin Institute of Technology, Shenzhen, China.*

[c] *Department of Materials Science and Metallurgy, University of Cambridge, Cambridge, United Kingdom*

[d] *College of Civil and Transportation Engineering, Shenzhen University, Shenzhen, China.*

[e] *School of Materials Science and Engineering, Southwest Jiaotong University, Chengdu, China.*

[f] *Research School of Electrical, Energy and Materials Engineering, Science, The Australian National University, ACT, Australia.*

[g] *Department of Engineering, Shenzhen MSU-BIT University, Shenzhen, China*

* *Corresponding authors and email address: zhongzheng@hit.edu.cn, qinghua.qin@smbu.edu.cn.*

This file includes:

Figures S1-S14.
Movie S1.
In situ bending test for a pillar with D=500 nm (speed up for seven times).
Movie S2.
In situ bending test for a pillar with D=300 nm (speed up for four times).
Movie S3.
In situ bending test for a pillar with D<300 nm (speed up for twelve times).
Movie S4.
Atomistic simulation of uniaxial compression on ZIF-62 glass with the dimension of 11.9 nm, 11.9 nm, and 13.84 nm.

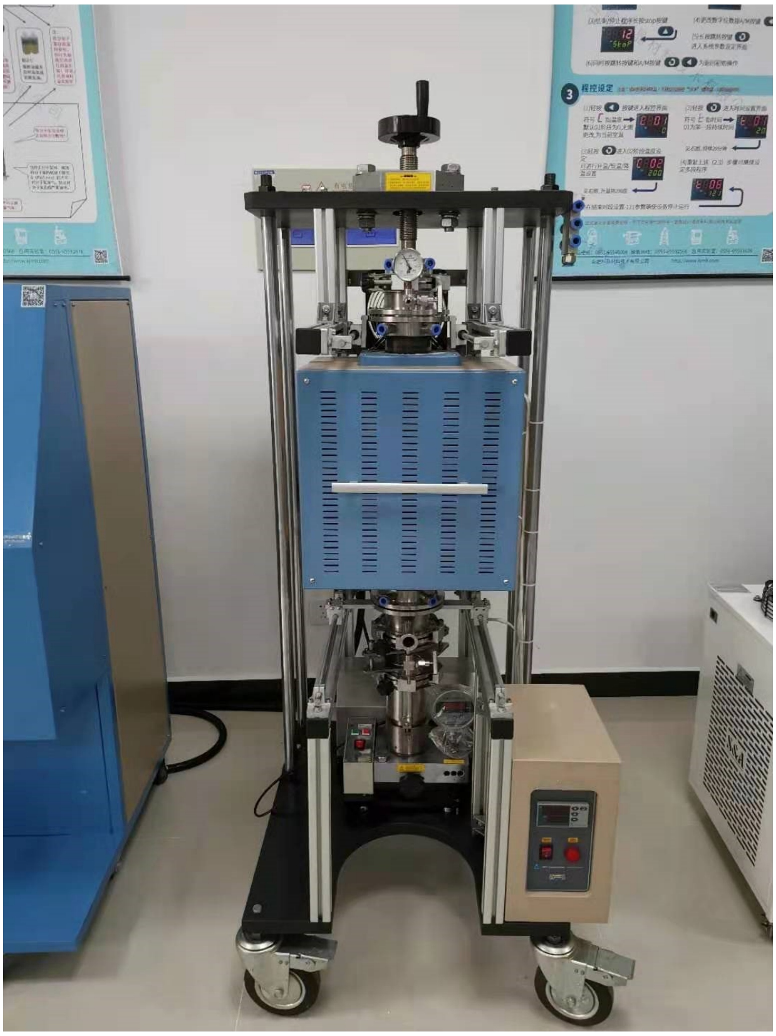

Figure S1. The hot-pressed machined used for fabricating ZIF-62 glass. The model is OTF-1200X-VHP4, more information can be found on the official website of Hefei Kejing Materials Technology Co., Ltd. (http://www.kjmti.com/product/14182.html).

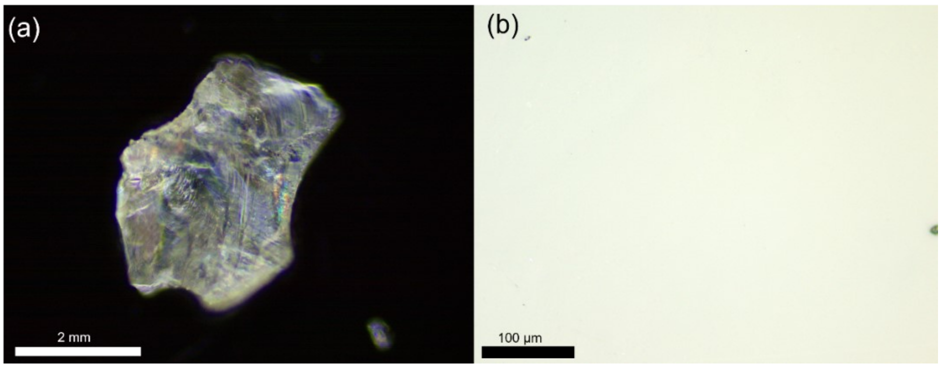

Figure S2. Optical observation of the ZIF-62 glass, (a) a piece of MOF glass, (b) no bubbles or cracks were seen under the microscopic examination.

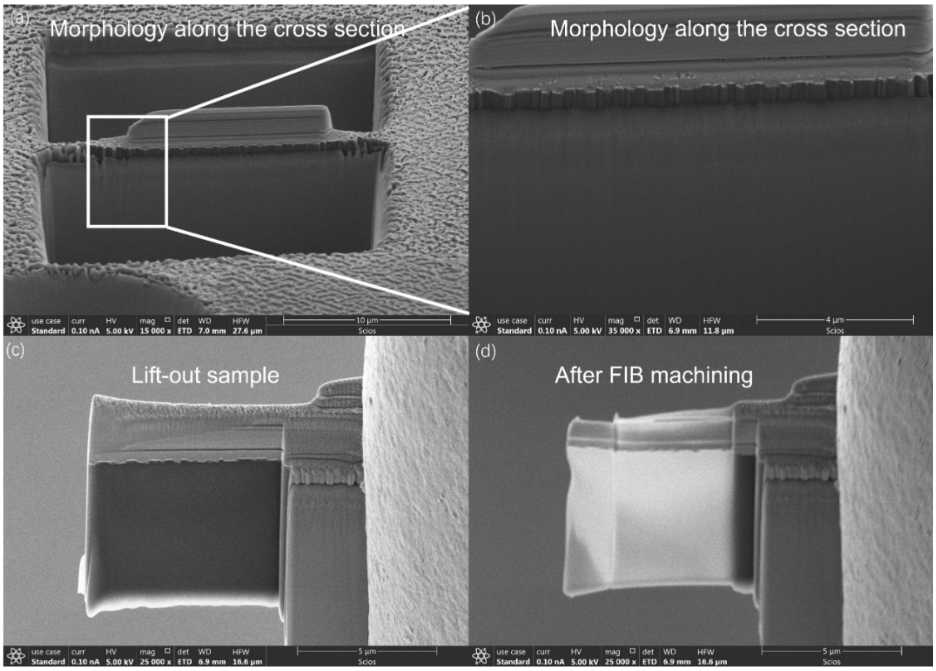

Figure S3. SEM observation along the cross section, no microscale bubbles/pores and cracks were evidenced in these figures.

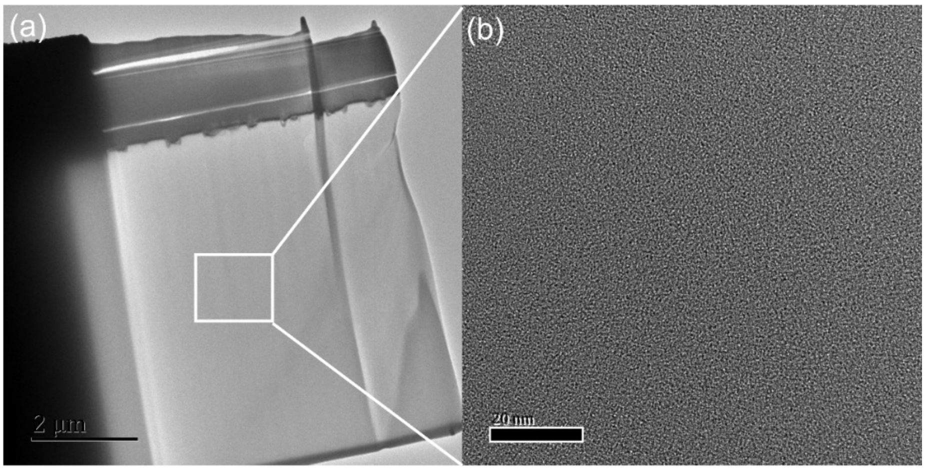

Figure S4. TEM examination along the cross section, the nanoscale observation shows no bubbles/pores and cracks in our sample.

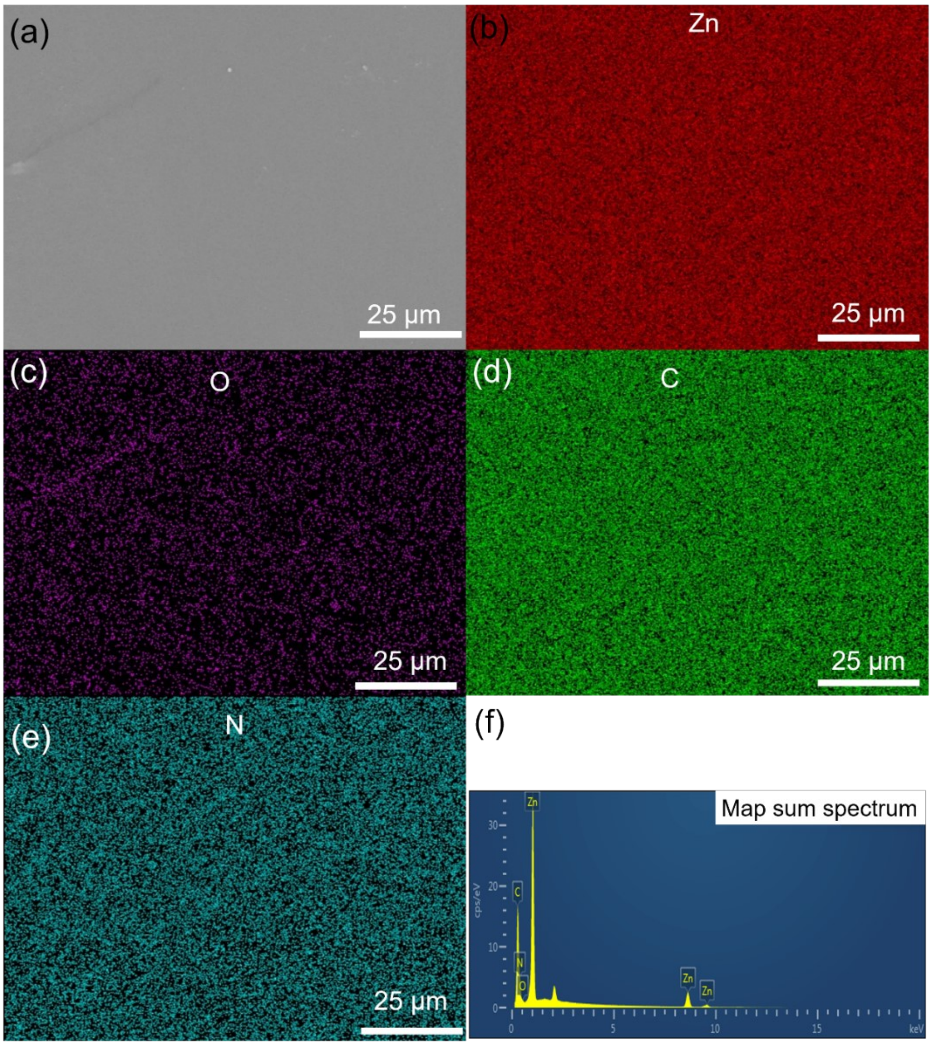

Figure S5. Distribution of chemical elements from the EDS observation in SEM. The elements were evenly distributed in our sample.

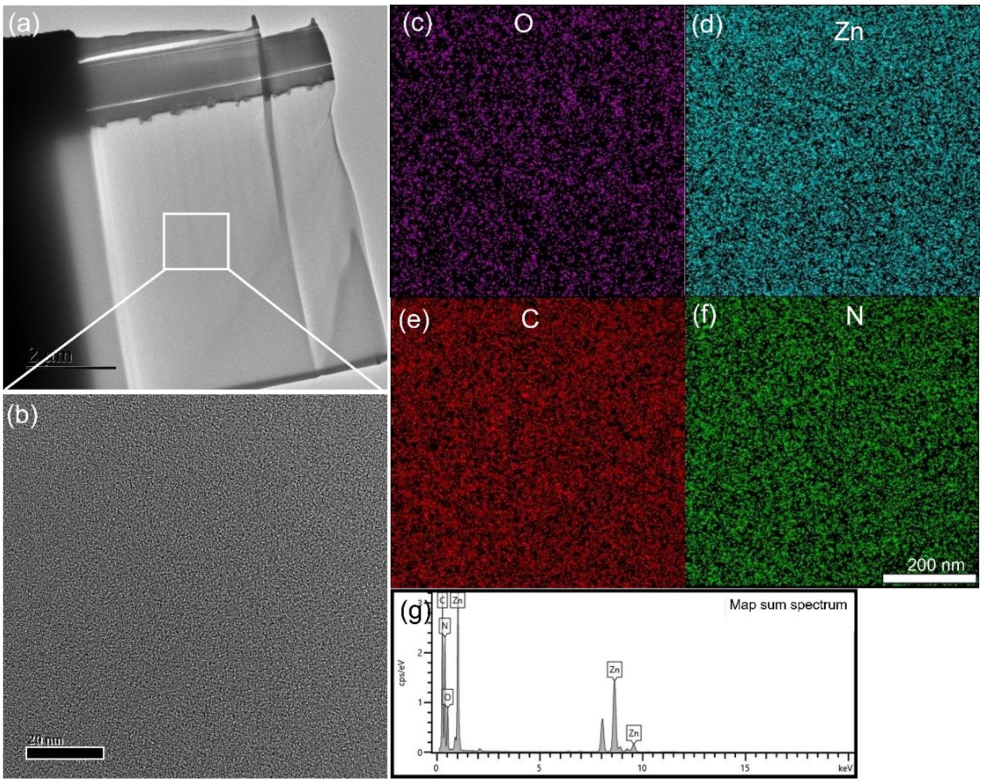

Figure S6. Nanoscale examination along the cross section in TEM, no cracks and bubbles/pores were presented, and the chemical elements were evenly distributed along the cross section.

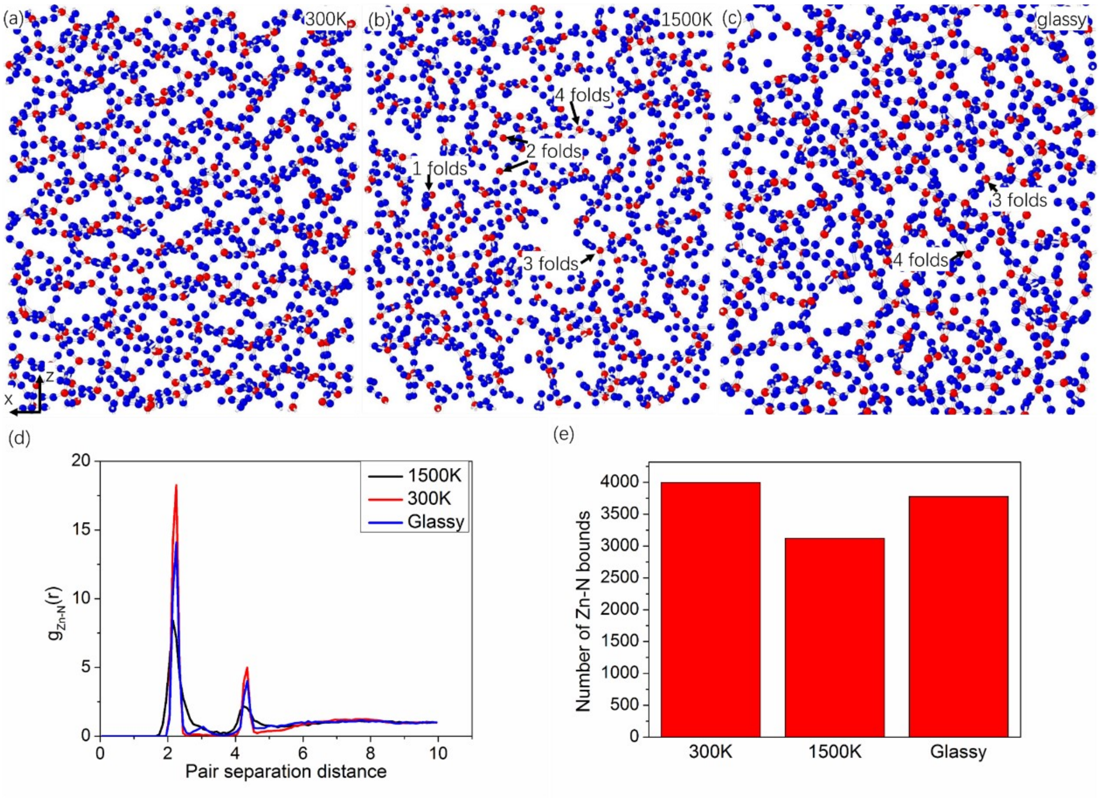

Figure S7. MD simulated microstructural changes in ZIF-62 during melt-quenched process. (a) 300 K, (b) 1500 K, (c) Glassy state. (d) Zn-N pair distribution function at different state. (e) The number of Zn-N bounds at different temperatures. At 300 K, most of Zn-N bonds are four-fold types; whereas the four-fold Zn-N bounds at 1500 K are broken into three-fold, two-fold, and one-fold ones, because Zn-N bounds tend to be separated at high temperatures. At glassy state, there are four-fold and three-fold Zn-N bonds, indicating that some Zn-N bounds reconnected during cooling down process.

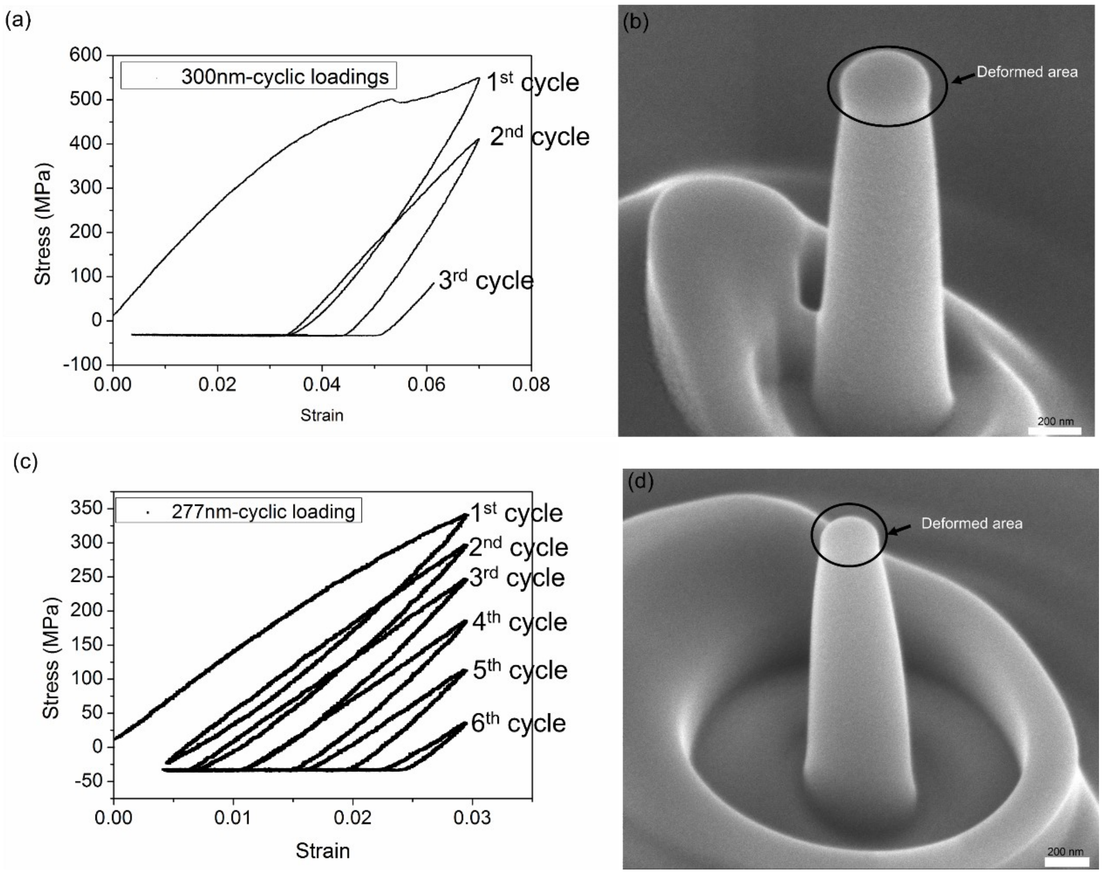

Figure S8. Cyclic loading on the pillars with D around 300 nm. (a) Cyclic stress-strain curves under 7% strains, softening behavior is presented from the curves. (b) SEM image shows that the deformed area locates at the top of the pillar, and deformation occurs in a ductile way. (c) Cyclic stress-strain curves under 3% strains, cyclic softening is also presented, though the applied strain is much smaller. (d) Ductile deformed morphology is shown in the SEM image.

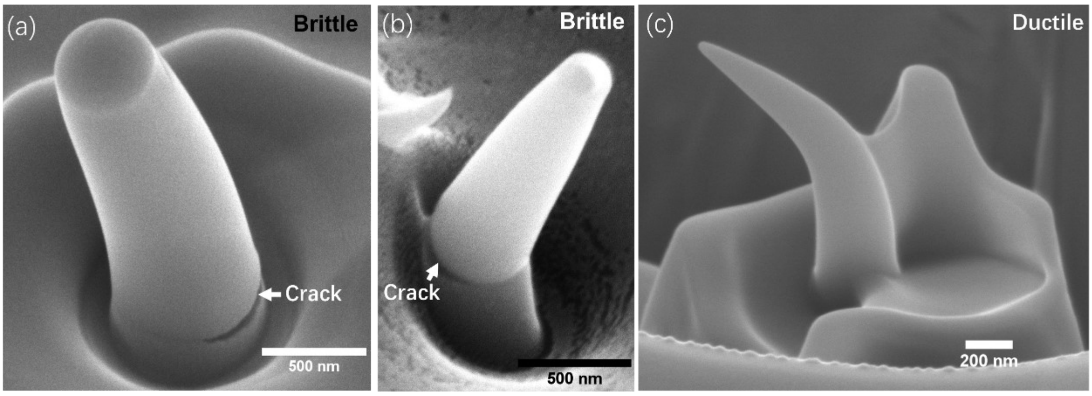

Figure S9. Brittle-to-ductile transition in pillars of ZIF-62 glass under in-situ mechanical testing. (a)-(c) The deformed morphologies of pillars with D=500 nm, 300 nm, and D≤100 nm, respectively. From (a)-(c), we can see that a transition from brittle state to ductile state is also observed in in-situ bending process. This figure confirms that the ZIF-62 glass can be deformed in a ductile way under tensile loadings when reducing the size below a critical value.

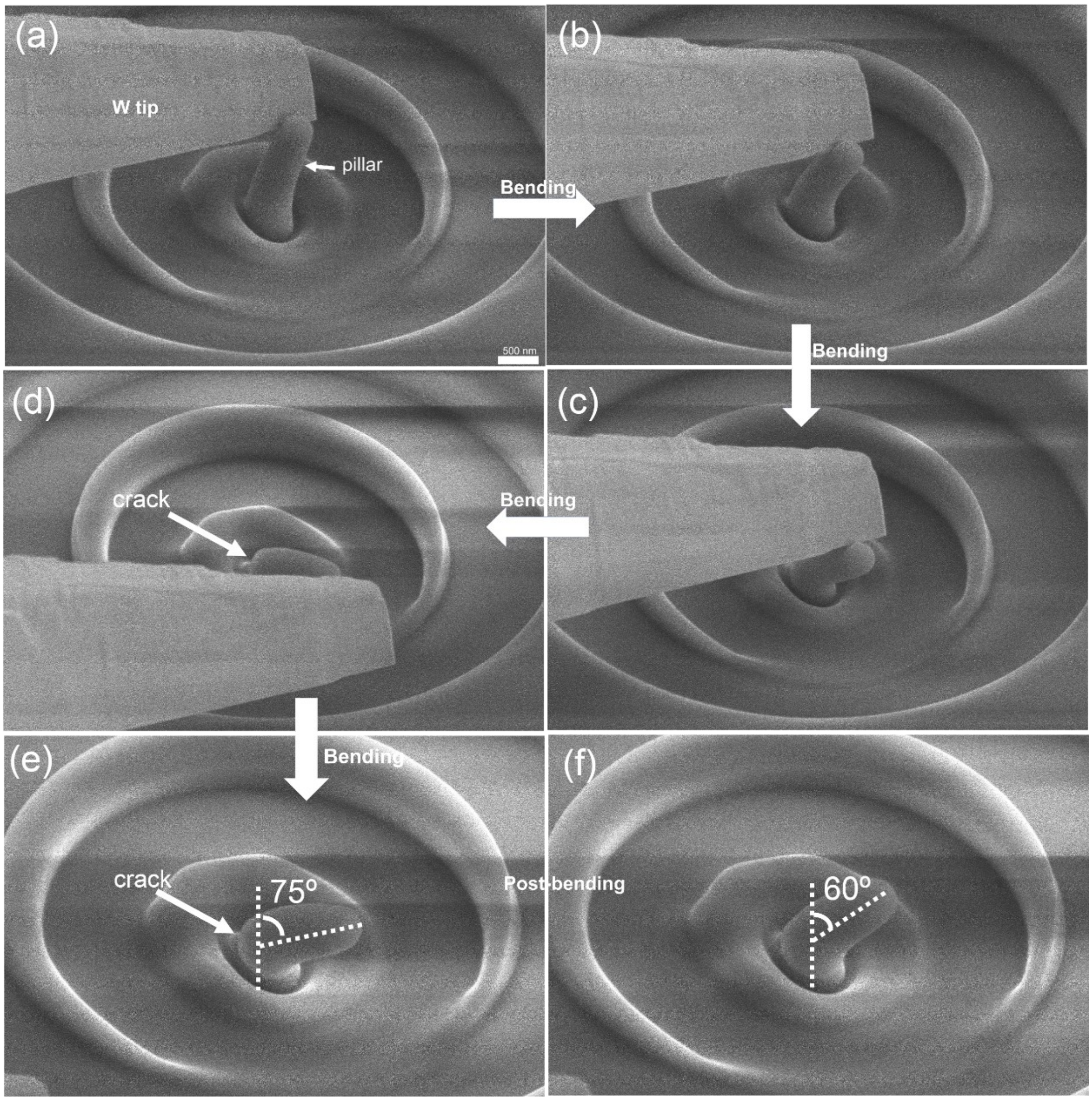

Figure S10. In-situ bending a pillar with D=500 nm. (a)-(d) Images showing that the pillar is bent with a W tip. The bottom (blue arrow indicated) is cracked during bending process. (e)-(f) SEM images show that the shape of the pillar recovers around 15º after unloading. This process indicates that the pillar with D=500 nm subjected to tensile stress fails in a brittle manner.

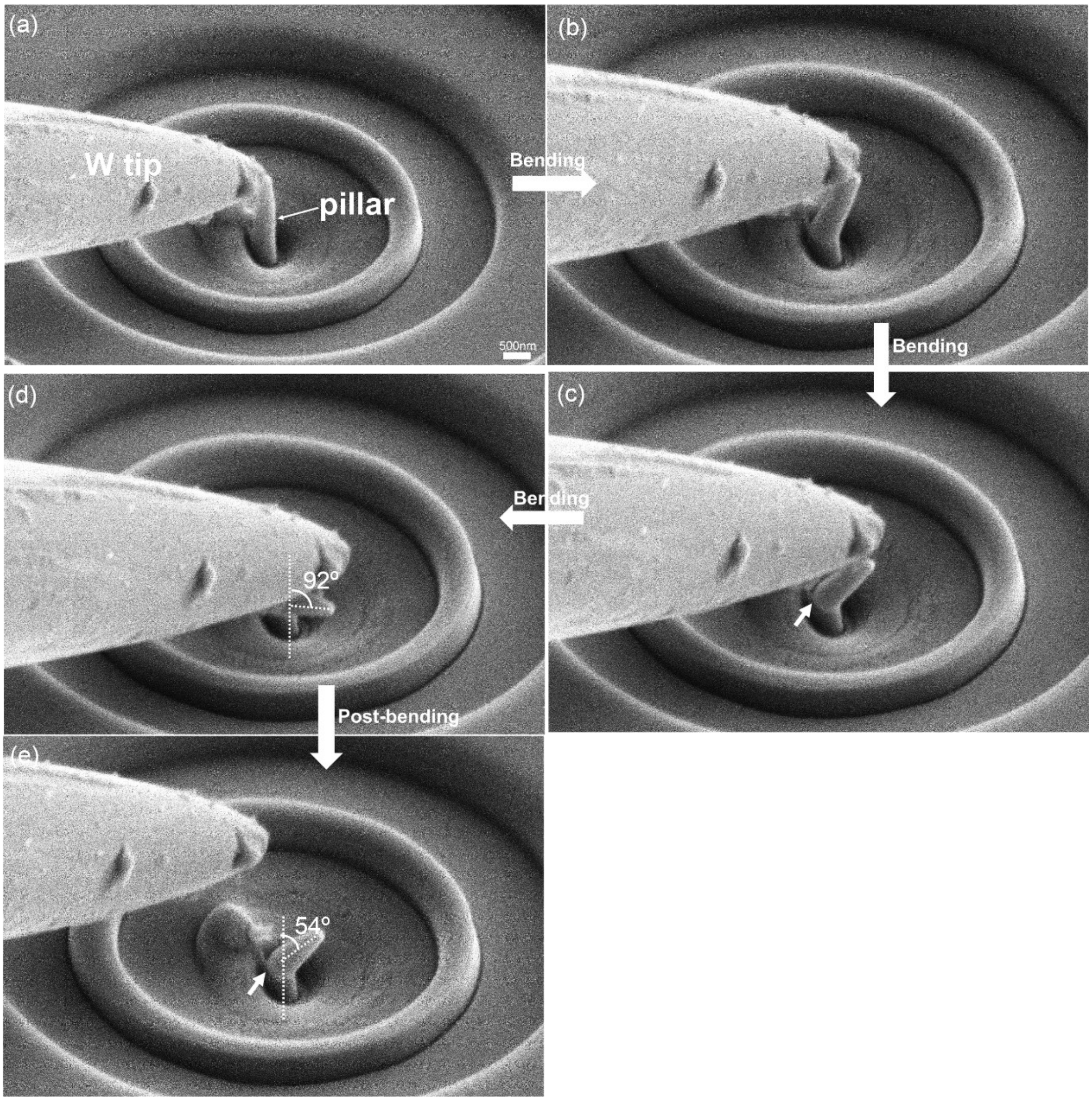

Figure S11. In-situ bending a pillar with D=300 nm. (a)-(d) SEM images show the in-situ bending process. Cracking occurs at the bottom (white arrow indicated in c). (d)-(e) SEM images show that the shape of the pillar recovers by 28º after unloadings. The crack at the bottom (white arrow indicated in c and e) suggests that the pillar with D=300 nm fails brittlely.

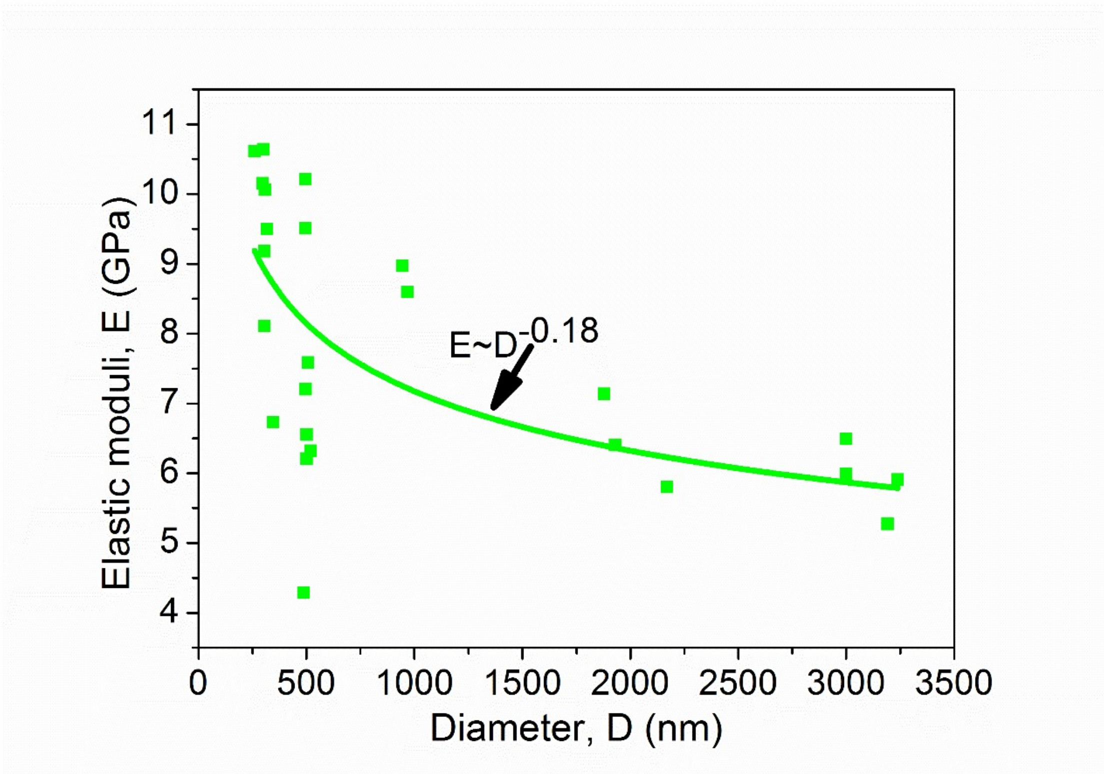

Figure S12. Plot of elastic modulus versus diameter, a trend of “smaller is stronger” is observed.

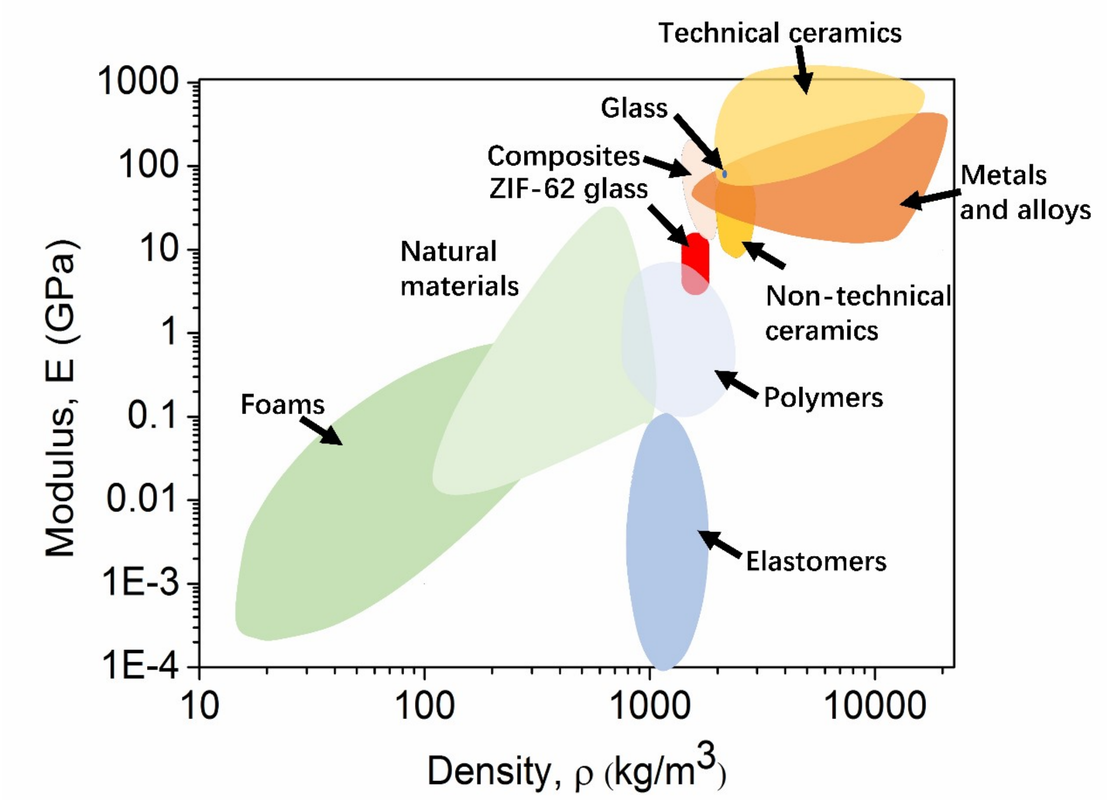

Figure S13. Ashby map of Young's modulus versus density of ZIF-62 glass and other structural materials. The modulus of ZIF-62 glass is overlapped with some non-technical ceramics, and greater than that of foams, polymers, elastomers, and most of natural materials. However, E of ZIF-62 glass is smaller than that of traditional glasses, technical ceramics, and metal alloys, due to the relative weakness of Zn-N bonds compared to others (e.g., Si-O).

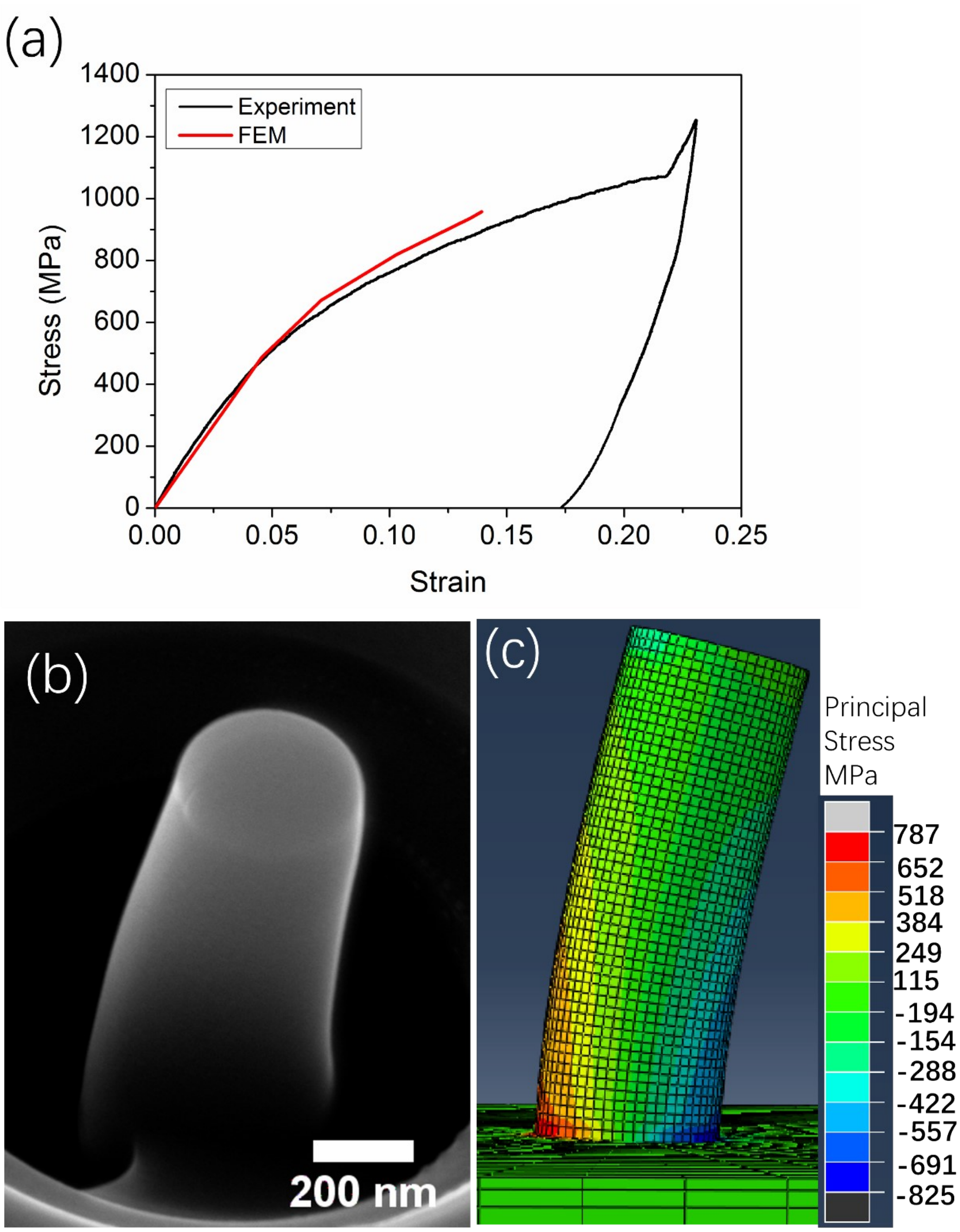

Figure S14. FEM simulation of bending a pillar (D=300 nm). (a) The stress-strain data from experiment and simulation, which shows a good fitting. (b) Deformed morphology of the bended pillar. (c) A similar morphology is attained from simulation, and the principal stress shows the distribution of tensile and compressive stress in the bended pillar.